e-ISSN: 2805-5756

PENERBIT PRESS
UNIVERSITI TEKNOLOGI MARA

Available online at
https://jaeds.uitm.edu.my

Journal of Applied Engineering Design and Simulation 6(2) 2026, 62–77

Journal of Applied Engineering Design and Simulation

Face-centred design approach for modelling and predicting areal surface roughness in freeform surface milling of stavax ESR

Mohd Faizal Yasak[1], Ahmad Faiz Zubair[1*], Mohd Fauzi Ismail[2], Muhammad Akmal Mohd Zakaria[1]

[1]*Faculty of Mechanical Engineering, Universiti Teknologi MARA Cawangan Pulau Pinang, Permatang Pauh Campus, 13500, Seberang Perai, Malaysia*
[2]*Faculty of Mechanical Engineering, Universiti Teknologi MARA, 40450, Shah Alam, Malaysia*

ARTICLE INFO

Article history:
Received 28 August 2026
Revised 17 September 2026
Accepted 22 September 2026
Online first 25 September 2026
Published 25 September 2026

Keywords:
Freeform surfaces
Face centered composite design
Ball nose milling
Stavax
ANOVA
Areal surface roughness

DOI:
10.24191/jaeds.v6i2.222

ABSTRACT

Freeform surfaces have become a major element in high precision industrial design, such as moulds and dies. These sculptured surfaces are characterised by non-uniform and aesthetic features requiring high-quality surface finishing. Therefore, minimising surface roughness becomes critical, especially when machining Stavax, a well-known material, in moulds and dies. This study aims to optimise 3-axis CNC ball nose milling parameters, namely spindle speed (v_c), feed rate (f_z), and depth of cut (a_p), in minimising areal surface roughness on the B-Spline tensor product of the Stavax freeform profile. A total of 17 experimental runs were designed using a face-centred composite approach (FCD) under the response surface methodology (RSM). Areal surface roughness data were captured via Alicona InfiniteFocus and then evaluated by MountainsLab in compliance with ISO 25178. ANOVA validation indicated a highly reliable predictive model, characterised by an R^2 of 0.9680, an adjusted R^2 of 0.9268, and a predicted R^2 of 0.8762 with the difference less than 0.2. This study also developed the FCD mathematical model for factors influencing the roughness.

[1*]Corresponding author. *E-mail address*: ahmadfaiz@uitm.edu.my

Nomenclature (Greek symbols towards the end)

v_c	spindle speed (rev/min)
f_z	feed rate (mm/min)
a_p	depth of cut (mm)
S_a	areal surface roughness (µm)
Ø	diameter (mm)

Abbreviations

CAD/CAM	computer aided design/computer aided manufacturing
CNC	computer numerical control
AISI	American Iron and Steel Institute
TiAlN	titanium aluminum nitrate
DOE	design of experiment
HRC	hardness Rockwell C
ESR	electroslag remelting

1. INTRODUCTION

Surface topography analysis has become a critical indicator in precision manufacturing, especially when involving mould and die machining. Surface-finish quality of the machined part and efficacy of the manufacturing are the main factors that influence the performance and durability of the final product [1]. In modern manufacturing, freeform surfaces are integral to the design and fabrication of diverse engineering components, particularly in the production of moulds and dies, aerospace, and energy industries [2]. For such demands, especially in mould and die manufacturing, Stavax has emerged as a preferred steel-based alloy due to its superior strength, corrosion resistance and exceptional thermal stability [3]. However, these properties create significant challenges during free form ball nose milling, particularly when a high-quality surface finish is required.

Milling machinings are broadly utilised in mould and die production to fabricate very detailed curved components with an acceptable surface finish and within dimensions [4]. According to Rashid et al. [4], in milling machining, ball nose mills are usually used in die manufacturing because they can achieve plane or freeform sculptured machining. Due to the industrial demand that requires excellent surface finishes, secondary finishing processes such as grinding, shot peening, sand blasting, polishing, and burnishing are employed after CNC machining [5]. Hence, attaining the specified surface finish is critical to reduce reliance on secondary finishing processes. As highlighted by Yıldız et al. [6], numerous studies have investigated the influence of various milling parameters to minimize surface roughness. Based on previous studies, the optimisation of CNC milling parameters, namely depth of cut, feed rate, and spindle speed, have a substantial outcome on Stavax freeform areal surface roughness.

CAD 3D software generates freeform surfaces using the boundary representation method that contains of topology and geometry. Topological elements, such as faces, edges, and vertices, describe the boundaries of a shape and establish hierarchical and connectivity associations among them [7]. In this case, B-splines are advantageous for both geometric design and mathematical modelling, specifically in defining complex geometries such as freeform surfaces [8-9]. The B-spline surface is defined using a tensor product representation, comprising an infinite array of B-spline curves oriented in two parametric directions [10].

Isoparametric curves along the *u*- or *v*-directions are constructed by holding the respective parameter constant. Because tensor product surfaces are mathematically derived from their constituent curves, the advantageous properties of individual B-spline curves are inherently transferred to the freeform surface [10]. Thus, in the present study, a tensor product B-spline algorithm was utilized in MATLAB to generate a freeform surface topology based on modern automotive bumper designs.

Response Surface Methodology (RSM) is an advanced statistical and mathematical approach used to explore the detailed interactions between independent parameters and response variables [11-12]. Face Centred Composite Design (FCD) is a variant of Central Composite Design (CCD) that is widely employed in response surface methodologies for experimental optimisation [13]. FCD provides an efficient statistical alternative to standard full-factorial designs by enabling the formulation of second-order (quadratic) models without requiring a comprehensive three-level factorial setup [13-14]. Benefiting from center and axial points that precisely model response surface curvature, a 17-run FCD was formulated in this study. This experimental setup evaluated combinations of spindle speed (v_c), feed rate (f_z), and depth of cut (a_p) to minimise areal surface roughness on the freeform surface of Stavax.

The arithmetical mean height S_a serves as the primary parameter to define and quantify areal surface roughness, as specified by the ISO 25178:2012 [15-16]. Unlike traditional profile roughness, which evaluates the surface along a single linear trace, areal surface roughness is computed by assessing the topographical data across a captured image by optical instruments [16]. The requisite ISO-standardised form removal and filtering for areal surface roughness are managed through default, automated workflows within metrology software such as Zygo Mx and MountainsLab [17-19]. Thus, it ensures accurate and consistent quantification of the areal surface roughness. Serving as a reference baseline, Kalisz et al. [19] reported that by utilising the Ø8 mm ball-end milling parameters (cutting speed = 350 m/min, feed = 0.04 mm, stepover = 0.53 mm, depth of cut = 0.5 mm) results in S_a = 2.67 µm on the concave surface and S_a = 2.71 µm on the convex surface.

Analysis of Variance (ANOVA) is a statistical method used to determine whether there are noteworthy variances in surface roughness among various groups or circumstances within an experiment, with *p*-values less than 0.05, indicating significant effects of process variables on surface roughness [20],[21]. To augment the ANOVA, three statistical metrics are used to evaluate the model fit, namely R^2, adjusted R^2, and predicted R^2 [11]. An elevated predicted R^2 confirms that the model generalizes effectively and accurately predicts new responses. Furthermore, when the R^2, adjusted R^2, and predicted R^2 values approach 1 with a variance of less than 0.2 between adjusted R^2 and predicted R^2, the model demonstrates reliability [11]. These evaluation metrics comprehensively validate the model's stability, ensuring it accurately captures inherent data patterns for reliable predictive performance [11].

2. METHODOLOGY

The experiment began by implementing B-spline curves in MATLAB to design the freeform surfaces. The freeform surface of Stavax in the current study replicated a subsection of the mould design that produces the aesthetic form of an automobile bumper. To optimise the machining of the Stavax surface, the 17 experimental runs were formulated using Stat-Ease's Design-Expert. A 3-axis CNC milling machine equipped with a Mitsubishi M70 controller was used to execute the scallop toolpath generated in CAD/CAM software. Alicona InfiniteFocus was employed to determine the areal surface roughness (S_a) of

the machined surface. Finally, statistical validation via ANOVA was performed to ascertain the individual significance of each machining parameter and derive the corresponding predictive model. Fig. 1 presents a detailed flowchart that outlines the steps of experimental methodology.

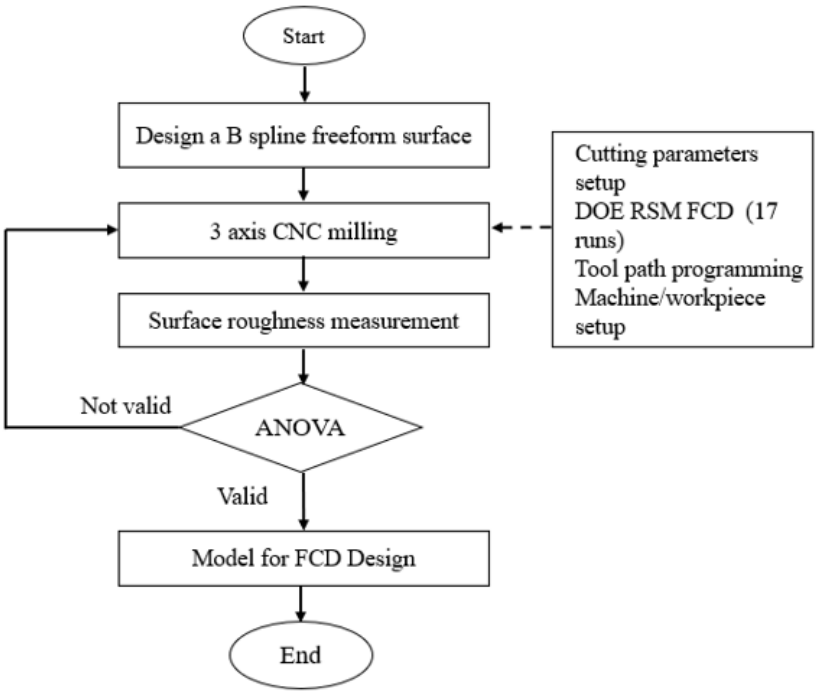


Fig. 1: The flowchart shows experimental procedures

2.1 Tensor product B-Spline surface formulation

The freeform surface generation algorithm is based on Tensor Product B-Spline formulation. This method constructs a parametric surface $S(u,v)$ by computing the tensor product of two single variable B-spline basis functions over a defining grid of control points. The general mathematical definition of a B-spline surface defined by polynomial degrees p and q along the u and v axes, respectively is given by Eq. (1):

$$S(u,v) = \sum_{i=0}^{n} \sum_{j=0}^{m} N_{i,p}(u) N_{j,q}(v) P_{i,j} \quad (1)$$

Where $S(u,v)$ is the Cartesian coordinate vector $[x(u,v), y(u,v), z(u,v)]^T$ of a point on the surface, $u, v \in [0,1]$ are the normalised parametric coordinates, $P_{i,j}$ represents the $(n+1) \times (m+1)$ grid of control points (cp) defining the hull of the surface and lastly $N_{i,p}(u)$ and $N_{j,q}(v)$ are the normalised B-Spline blending functions of degree p and q respectively. In the implementation, a quadratic surfce is generated $(p = q = 2)$ using a 3×3 control point grid $(n = m = 2)$.

The base functions $N_{i,p}(u)$ are computed recursively using the Cox-de Boor algorithm, which ensures numerical stabilility.
Base case (p = 0):

$$N_{i,0} = \begin{cases} 1 & if\ u_i \le u < u_{i+1} \\ 0 & otherwise \end{cases} \quad (2)$$

Recursive step ($p > 0$):

$$N_{i,p}(u) = \frac{u-u_i}{u_{i+p}} N_{i,p-1}(u) + \frac{u_{i+p+1}-u}{u_{i+p+1}-u_{i+1}} N_{i+1,p-1}(u) \quad (3)$$

The knot vector U determines the topology of these functions. For this study, an open uniform (clamped) knot vector was utilised to ensure the surface interpolates the boundary control points: $U = V =$ {0,0,0,1,1,1}. A critical requirement of this is the precise control of the surface's maximum depth at a shifted location. The necessary control point in vertical position (P_z) was derived to achieve a specific target depth (Z_{target}) at the geometric center (u = 0.5, v = 0.5). For a quadratic B-Spline with knot vector {0,0,0,1,1,1}, the base functions correspond to Bernstein polynomials. The value of the central basis function (i = 1) at (u = 0.5) is derived in Eq. (4):

$$N_{1,2}(0.5) = 2u(1-u)\,\big|_{u=0.5} = 2(0.5)(0.5) = 0.5 \quad (4)$$

The surface depth $Z(u,v)$ at the center is the tensor product sum of the control points' Z-coordinates $\left(Pz_{i,j}\right)$. By using the Eq. (1), it becomes:

$$(0.5,0.5) = \sum_{i=0}^{2} \sum_{j=0}^{2} N_{i,2}(0.5) N_{j,2}(0.5) Pz_{i,j} \quad (5)$$

Since the boundary/rim control points are constrained to Z = 0, only the central control point $Pz_{i,j}$ is non-zero. Hence, the equation simplifies to:

$$Z(0.5,0.5) = N_{1,2}(0.5) N_{1,2}(0.5) Pz_{1,1} \quad (6)$$

In order to solve the height of the control point, substitute the simplified Eq. (6) in Eq. (4) which gives:

$$Z_{target} = (0.5)(0.5) Pz_{1,1} \quad (7)$$

Rearrange Eq. (7) to solve the required control point height:

$$Pz_{1,1} = \frac{Z_{target}}{0.25} \quad (8)$$

If the surface depth is Z_{target} = -2.0 mm hence, the central control point must be positioned at Z = -8.0 mm. As a result, the surface size of 18 mm × 15 mm × 2 $mm\ depth$ was created as shown in Fig. 2.

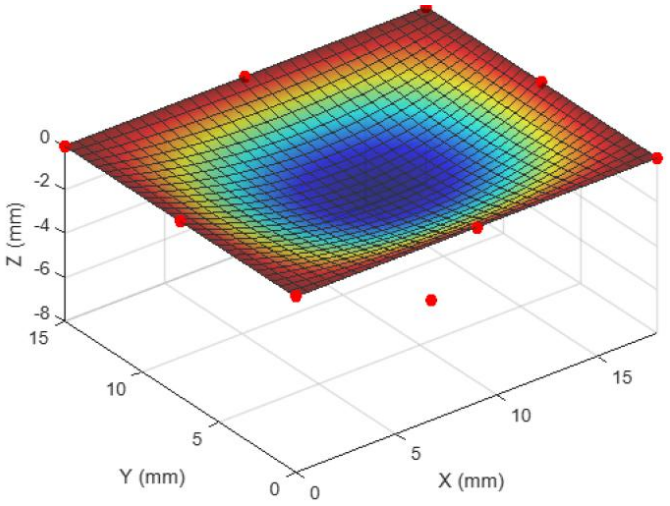


Fig. 2: MATLAB-generated B-spline surface representing the subsection of automotive bumper mould

2.2 Face Centred Composite design (FCD)

Regarding the process parameters, the study evaluated three specific independent factors: spindle speed (v_c), feed rate (f_z), and depth of cut (a_p). The parameters were determined based on existing literature and experimental data [22-23]. The range for these parameters is rigorously established based on the tool manufacturer's recommended cutting data for CNC milling of pre-hardened steel, as listed in Table 1.

Table 1: Cutting parameters for a 6 mm TiAlN-coated carbide dual-flute ball-nose end mill

Parameter	**Unit**	**Lower Level (-1)**	**Middle Level (0)**	**Upper Level (+1)**
Spindle Speed	rpm	2560	3200	3840
Feed Rate	mm/min	144	180	216
Depth of Cut	mm	0.1	0.2	0.3

Based on the experimental design of Design-Expert RSM Face-Centred Composite (FCD), a total of 17 assessments need to be conducted. Each parameter was systematically varied across three discrete levels, namely low, centre, and high, to evaluate their individual and interactive effects. The experimental matrix included three replications at the median parameter levels, utilising a spindle speed of 3200 rpm, a feed rate of 180 mm/min, and a depth of cut of 0.2 mm. These centre point runs were integrated to estimate pure experimental error, assess machine repeatability, and allow the ANOVA to test for significant curvature in the response surface model.

2.3 Programming and machining

The surface size of 18 mm × 15 mm × 2 $mm\ depth$ was matched with Ø6 mm TiAlN-coated carbide dual-flute ball nose milling on Stavax. The modified AISI420 is a fine stainless mould steel for small and

medium inserts and cores that integrate corrosion and wear sturdy with outstanding polishability, decent machinability and stability in hardening [24]. The author limited the study to a shallow concave surface while maintaining B-Spline free-form and aesthetic characteristics. While the size of the experimental surface is relatively minuscule compared to any actual product, one must agree that there are a number of experiments that must be conducted based on the Face Centered Composite Design (FCD). In the CNC machining, an experienced programmer prioritizes machining cycle time together with aesthetic view. Furthermore, the optical 3D surface roughness measurement tester, Alicona InfiniteFocus only requires a path length below 3 mm to summarise the areal surface topology. Following the selection of Ø6 mm TiAlN-coated carbide dual-flute ball nose milling, the author also made reference from Xie et al. [25] and Sun et al. [26]. In their studies, the size of the radius of ball nose directly affected the surface roughness during machining. With a bigger tool radius, a CNC programmer can increase the spindle speed, use a deeper depth of cut and use a faster feed rate; hence, lower the cycle time. However, the tool radius must be lower than the curvature of the surface to avoid overcut and ensure the precision of the shape as per design.

CNC programs were generated using Autodesk Fusion to execute the 17 experimental runs defined by the FCD. For each experiment, the specific levels of spindle speed (v_c), feed rate (f_z), and depth of cut (a_p) were integrated into the toolpath parameters within the CAM environment. Given the geometry of the free-form surface, the 3D pocket clearings were employed as a roughing strategy for clearing unwanted materials from the surface, leaving from 0.1mm to 0.3 mm of a thin layer as a finishing clearance as shown in Fig. 3. The toolpath strategy utilised flood coolant and a Ø6 mm TiAlN-coated carbide dual-flute carbide ball nose mill with an inclination angle of 10^0. Tool inclination evades the non-cutting region in the centre of the tool, thus preventing ploughing [2],[26]. The Ø6 mm TiAlN-coated carbide dual-flute ball nose mill with a 30° helix angle is effective for machining pre hardening Stavax ESR at hardness levels below 48 HRC. The TiAlN coating provides the necessary thermal stability and wear resistance during the milling of free-form surfaces [28]. In the finishing strategy, the step distance was fixed at 0.2 mm for all 17 experiments. A new Ø6 mm TiAlN-coated carbide dual-flute ball nose mill was utilised for each individual run to negate the effects of tool wear on surface roughness and ensure experimental consistency.

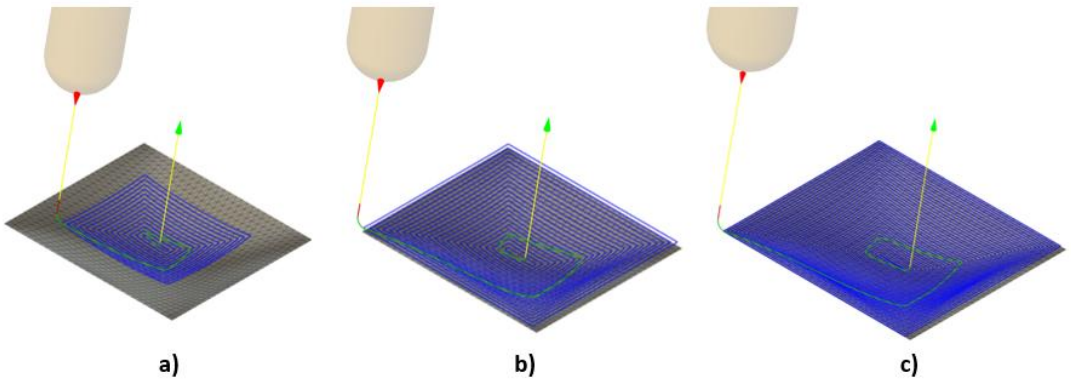


Fig. 3: Cutting simulation of scallop toolpath for ball-nose end milling. a) Roughing b) Semi finishing c) Finishing

While the 3-axis CNC milling worktable was capable of supporting the initial 50 mm × 200 mm × 30 mm Stavax workpiece, sectioning the material was necessary because the full block exceeded the weight limitations of the focus variation microscope platform. Therefore, the initial 200 mm long workpiece was sectioned into four individual blocks, each with dimensions of 50 mm × 50 mm × 30 mm. To accommodate

17 experimental trials proposed by the face-centred composite design (FCD), each block was subdivided into four equal 18 mm × 15 mm machining areas on its top surface. This configuration yielded 16 machined surfaces. The remaining trial was subsequently executed on the opposite surface of one of the blocks. Based on the density of Stavax, the weight of each sample was approximately 0.585 kg.

2.4 Areal surface roughness measurement

The Alicona InfiniteFocus non-contact microscope (Alicona Imaging GmbH,Austria), utilizing the focus variation principle, was used to measure the areal surface roughness of the machined Stavax surface. It has been utilised as a multipurpose measurement tool for various industries, with its high-resolution, non-contact measurement capabilities supporting both process optimisation and quality assurance [28-30].

The process to determine the areal surface roughness is shown in Fig. 4. The microscope captured a field of view measuring 2.85 mm × 2.16 mm at 10x magnification. Areal surface roughness was extracted from the non-contact profilometer measurements by applying the steps outlined in ISO 25178-2:2021. MountainMap® was used to analyse the image. In the beginning, the raw data, representing the primary topography, was initially leveled using a least squares plane (LSPL) operator to establish a horizontal reference baseline. Then, the software removed the form (F-operation) by applying a least squares polynomial of the 3rd degree (LSP3) to flatten the data [32]. A 3rd-degree polynomial is highly effective for isolating roughness on machined freeform surfaces. Then, a standard Gaussian filter was applied with a cut-off length of 0.8 mm [32]. Any surface undulations with a wavelength longer than 0.8 mm are classified as waviness, and those shorter than 0.8 mm are classified as actual surface roughness.

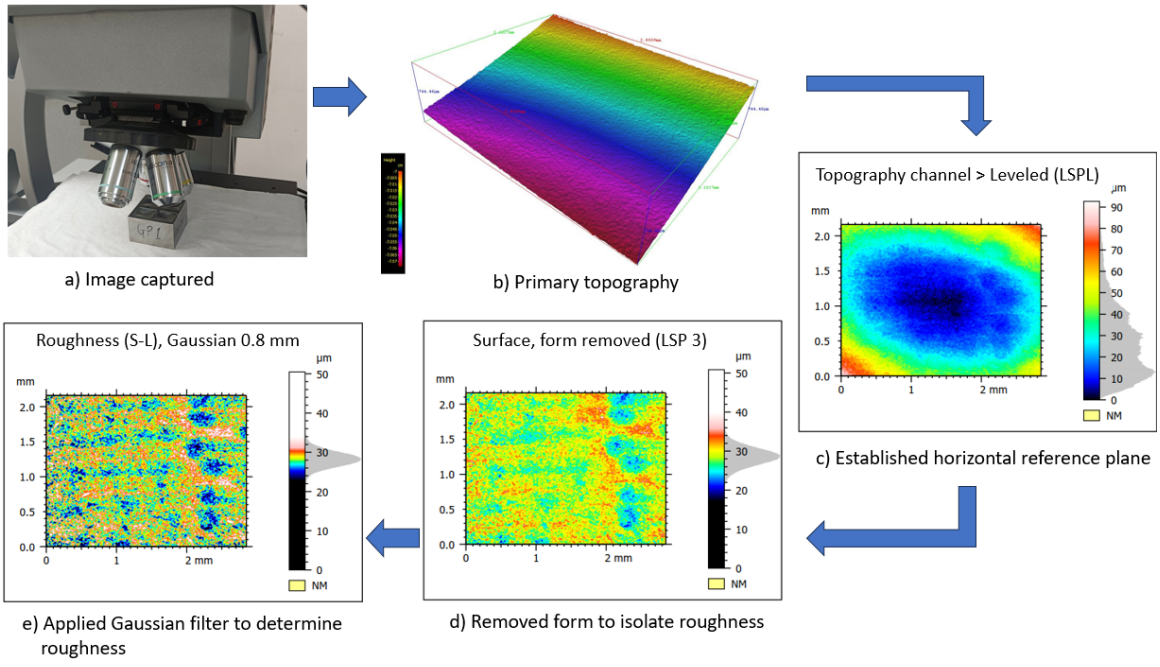


Fig. 4: Steps in measuring areal surface roughness

3. RESULTS AND DISCUSSION

3.1 Analysis of Variance

ANOVA, as a part of response surface methodology, is utilised to calculate *p*-values in order to verify that magnitudes of spindle speed, feed rate, and depth of cut are statistically significant. The areal surface roughness (S_a) data gathered from the 17 experimental trials are tabulated in Table 2. These data are utilised to develop a statistically significant predictive model.

Based on Table 3, the predictive model was determined to be highly significant, evidenced by an *F*-value of 23.52 and a *p*-value of 0.0002. Terms with *p*-values below 0.05 are considered statistically significant [32],[33]. According to ANOVA analysis, cutting parameters *A* (spindle speed) and *C* (depth of cut) significantly influence the areal surface roughness. The validity of the model was further confirmed by an insignificant lack-of-fit *F*-value of 1.41; thus, the predicted values are in strong agreement with the observed responses and not heavily influenced by noise.

Table 2: Measured surface roughness under varying spindle speed, feed rate, and depth of cut

Run	Spindle Speed (rev/min)	Feed Rate (mm/min)	Depth of Cut (mm)	Areal Surface Roughness (µm)
1	3840	144	0.1	1.682
2	3200	216	0.2	2.642
3	3840	180	0.2	2.172
4	3200	180	0.2	2.387
5	2560	144	0.1	2.294
6	3200	180	0.1	2.155
7	3200	180	0.3	2.962
8	2560	216	0.1	2.557
9	2560	144	0.3	3.310
10	3200	180	0.2	2.509
11	3840	144	0.3	2.349
12	2560	180	0.2	3.065
13	3200	180	0.2	2.280
14	3840	216	0.1	1.759
15	3840	216	0.3	2.373
16	2560	216	0.3	3.457
17	3200	144	0.2	2.560

3.2 Response Surface between Milling Parameters and Areal Surface Roughness

The validity of response surface model was confirmed by the normal probability plot of the externally studentised residuals in Fig. 5a. The close conformity of the studentised residual points to the straight diagonal line confirmed that the error distribution is approximately normal. The model exhibited consistent predictive accuracy across the entire experimental design space, as evidenced by the uniform dispersion of the surface roughness values of 1.682 to 3.457 µm along the normal probability line. Fig. 5b illustrates the

residuals versus predicted plot for confirming homogeneity of variance. While a slight vertical clustering of residuals was observed near the center of the design space, the overall dispersion lacked any severe structural patterns, such as a distinct funnel shape. All residual points fell safely within the upper and lower control limits of 4.81963, satisfying the assumption of constant variance and validating the model's adequacy.

Table 3: Analysis of variance (ANOVA) for assessing model significance of areal surface roughness of Stavax freeform machining.

Source	Sum of Squares	df	Mean Square	*F*-value	*p*-value	
Model	3.60	9	0.4000	23.52	0.0002	**significant**
A-Spindle speed	1.89	1	1.89	111.17	< 0.0001	
B-Feed rate	0.0034	1	0.0034	0.1977	0.6700	
C-Depth of cut	1.60	1	1.60	94.28	< 0.0001	
AB	0.0119	1	0.0119	0.7018	0.4298	
AC	0.0504	1	0.0504	2.96	0.1288	
BC	0.0036	1	0.0036	0.2099	0.6607	
A^2	0.0015	1	0.0015	0.0865	0.7772	
C^2	0.0044	1	0.0044	0.2567	0.6280	
A^2B	0.0008	1	0.0008	0.0492	0.8307	
Residual	0.1190	7	0.0170			
Lack of Fit	0.0928	5	0.0186	1.41	0.4637	**not significant**
Pure Error	0.0263	2	0.0131			
Cor Total	3.72	16				

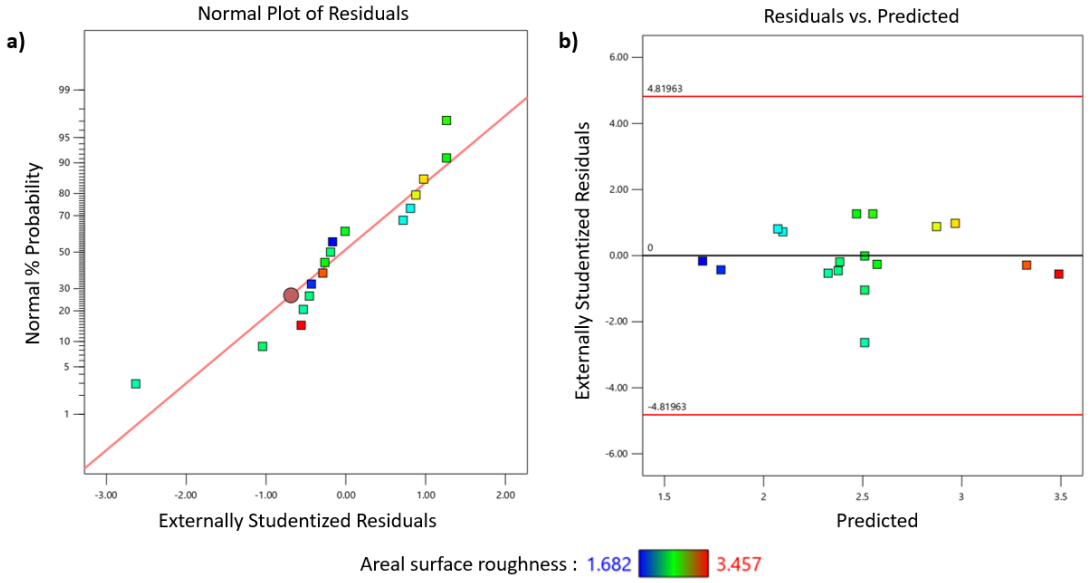


Fig. 5: Model adequacy diagnostic plots for areal surface roughness: a) normal probability plot, and b) residuals versus predicted plot.

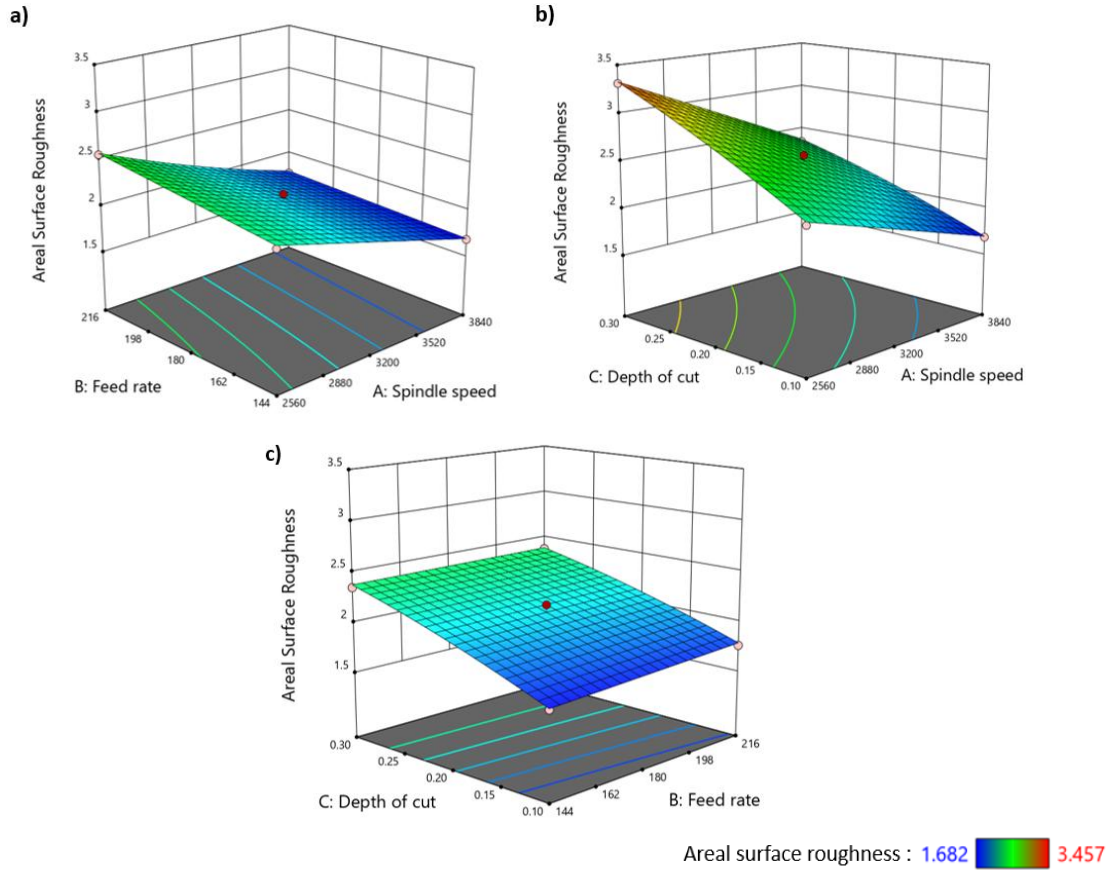


Fig. 6: 3D response surface plot for areal surface roughness as a function of a) feed rate and spindle speed b) depth of cut and spindle speed c) depth of cut and feed rate

Fig. 6a illustrates the linear 3D response surface plot of spindle speed and feed rate on areal surface roughness, evaluated at a constant depth of cut. The plot illustrated the lowest areal surface roughness ($S_{a)}$ when maintaining a constant depth of cut of 0.10 mm. The graph also indicated that spindle speed has a significant inverse relationship with areal surface roughness. For the Ø6 mm TiAlN-coated carbide dual-flute ball-nose mill, increasing the spindle speed from 2560 to 3840 rpm resulted in a significant reduction in areal surface roughness of freeform Stavax ESR. In another way, increasing the feed rate from 144 to 216 mm/min led to a gradual deterioration in surface finish. The topography of the response surface demonstrated that the minimum S_a= 1.682 µm is achieved at the maximum spindle speed of 3840 rev/min and the minimum feed rate of 144 mm/min.

Fig. 6b illustrates an inverse relationship between spindle speed and areal surface roughness, evaluated at a constant feed rate of 144 mm/min. As illustrated by the plot, maintaining this constant feed rate produces the lowest areal surface roughness. The topography of the plot revealed the lowest S_a= 1.682 µm when maintaining the highest spindle speed of 3840 rev/min coupled with the lowest depth of cut of 0.10 mm. Visually, the response surface revealed that the gradient along the depth of cut axis is slightly steeper than that of the spindle speed. This indicates that the depth of cut has a slightly greater effect on the areal

surface roughness (S_a) of the freeform Stavax ESR than the spindle speed when utilising the Ø6 mm TiAlN-coated carbide dual-flute ball-nose mill.

Figure 6c illustrates the interactive effect of feed rate and depth of cut on areal surface roughness (S_a), evaluated at a constant spindle speed. The plot illustrated the lowest areal surface roughness (S_a) when maintaining a constant spindle speed of 3840 rev/min. The minimum areal surface roughness S_a= 1.682 µm was achieved only when combining the minimum feed rate and depth of cut, which are 144 mm/min and 0.1 mm, respectively. Moreover, the plot revealed that the gradient along the depth of cut axis is significantly steeper than that of the feed rate axis. Thus, it confirmed the dominant effect of depth of cut on the areal surface roughness (S_a) for the Ø6 mm TiAlN-coated dual-flute ball-nose mill

3.3 Regression Model of Areal Surface Roughness

The areal surface roughness (S_a) regression model for the freeform machining of Stavax ESR utilising Ø6 mm TiAlN-coated carbide dual-flute ball-nose mill is presented in Eq. (9). However, the relative influence of each machining parameter cannot be directly compared using these coefficients, as they are inherently scaled to accommodate different measurement units. Instead, the relative significance and dominant effect of each parameter were determined by evaluating their respective *F*-values within the ANOVA framework as presented in Table 3. In the Eq. (9), S_a is areal surface roughness, *A* is spindle speed (rpm), *B* is feed rate (mm/min), and *C* is depth of cut (mm).

$$S_a = -0.752574 + 0.0013132A + 0.0235625B + 10.5475C - 1.16048 \times 10^{-5}AB - 0.00124023AC - 0.00586806BC - 2.25433 \times 10^{-7}A^2 - 3.79623C^2 + 1.55131 \times 10^{-9} A^2B \quad (9)$$

Subsequent fit statistics, detailed in Table 4, confirm the robust predictive capability of the formulated model. The model demonstrated strong predictive capability, with the predicted R^2 = 0.8762 being in close agreement with the adjusted R^2 = 0.9268 while the difference between them is <0.2. The value of nearly 1.0 indicates the best possible correlation between surface roughness and process variables [16-17]. Furthermore, an adequate precision value of 17.979 confirms a sufficient signal-to-noise ratio, indicating that the regression model can accurately predict the areal surface roughness (S_a) of the freeform Stavax ESR based on the evaluated combinations of spindle speed, feed rate, and depth of cut.

Table 4: Evaluation criteria of the model

Std. Dev.	Mean	C.V. %	R^2	Adjusted R^2	Predicted R^2	Adeq Precision	The Difference
0.1304	2.50	5.21	0.9680	0.9268	0.8762	17.9786	0.0506

4. CONCLUSION

This study investigated the optimisation of spindle speed, feed rate, and depth of cut to minimise the areal surface roughness (S_a) during the freeform milling of Stavax ESR using a 6 mm TiAlN-coated carbide dual-flute ball-nose mill. The ANOVA results dictate that the spindle speed is the most significant parameter influencing surface finish followed closely by depth of cut. The minimum areal surface

roughness S_a = 1.682 µm, is achieved by applying a minimal depth of cut of 0.10 mm, feed rate of 144 mm/min alongside a spindle speed of 3840 rev/min. A regression model was successfully developed to establish the mathematical relationship between these machining parameters and the machined Stavax ESR surface roughness. Statistical validation confirms the high reliability of this equation, yielding a predicted coefficient of determination, R^2 = 0.8762. As this value substantially exceeds the 0.80 threshold for strong correlation, the formulated model can be confidently utilized to predict surface roughness in the freeform milling operations of Stavax ESR. Furthermore, this empirical model can serve as the objective function within metaheuristic optimization algorithms to systematically determine the optimised cutting parameter combinations required to minimise areal surface roughness (S_a).

5. ACKNOWLEDGEMENTS/FUNDING

The authors would like to thank the Ministry of Higher Education Malaysia, Department of Education Polytechnics and Community Colleges, Universiti Teknologi MARA Shah Alam, Universiti Teknologi MARA Cawangan Pulau Pinang, Kolej Komuniti Kepala Batas and Kolej Komuniti Taiping for the resources and facilities used throughout the research.

6. CONFLICT OF INTEREST STATEMENT

The authors declare that they have no known competing financial interests or personal relationships that could have appeared to influence the work reported in this paper.

7. AUTHORS' CONTRIBUTIONS

Mohd Faizal Yasak: Conceptualization, methodology, investigation (execution of primary experiments), data curation, validation, writing (original draft).

Ahmad Faiz Zubair: conceptualization, supervision, project administration, funding acquisition, resources, writing (review and editing).

Mohd Fauzi Ismail: Investigation and formal analysis (topology and measurement surface).

Muhammad Akmal Mohd Zakaria: Formal analysis (RSM and Anova) and validation.

8. DECLARATION OF GENERATIVE AI IN THE WRITING PROCESS

During the preparation of this work, the author used GEMINI AI to improve the readability and language quality of the manuscript. After using this tool, the author reviewed and edited the content as needed and take full responsibility for the content of the publication.

9. DATA AVAILABILITY/SUPPLEMENTARY MATERIALS

All data generated or analysed during this study are included in this published article.

10. ETHICS STATEMENT

The authors declare that this research did not involve human or animal subjects.

11. REFERENCES

[1] P. N. Linh, T. N. Tan, V. D. Toan, and T. D. Nguyen, 'Multi-Objective Optimization of Finishing Milling of C45 Steel using Factorial Design', *Eng. Technol. Appl. Sci. Res.*, vol. 14, no. 6, pp. 18199–18204, 2024, doi: 10.48084/etasr.8017.

[2] F. Marin, A. Fagali De Souza, H. Da Silva Gaspar, A. Calleja-Ochoa, and L. N. López De Lacalle, 'Topography simulation of free-form surface ball-end milling through partial discretization of linearised toolpaths', *Eng. Sci. Technol. Int. J.*, vol. 55, p. 101757, 2024, doi: 10.1016/j.jestch.2024.101757.

[3] S. Maeng, H. Ito, Y. Kakinuma, and S. Min, 'Study on Cutting Force and Tool Wear in Machining of Die Materials with Textured PCD Tools Under Ultrasonic Elliptical Vibration', *Int. J. Precis. Eng. Manuf.-Green Technol.*, vol. 10, no. 1, pp. 35–44, 2023, doi: 10.1007/s40684-022-00416-0.

[4] M. F. M. Rashid, M. H. A. Bakar, M. F. Mamat, N. A. Rosli, N. A. Wahab, and S. G. Herawan, 'Optimization of Cutting Parameters for Surface Roughness and Microscopy Analysis in Machining Hardened High Thermal Conductivity 150 (htcs-150) Steel', *Malays. J. Microsc.*, vol. 20, no. 2, pp. 133–144, 2024.

[5] D. Masato and S. K. Kim, 'Global Workforce Challenges for the Mold Making and Engineering Industry', *Sustainability*, vol. 16, no. 1, p. 346, 2023, doi: 10.3390/su16010346.

[6] A. Yıldız, L. Uğur, and İ. E. Parlak, 'Optimization of the Cutting Parameters Affecting the Turning of AISI 52100 Bearing Steel Using the Box-Behnken Experimental Design Method', *Appl. Sci.*, vol. 13, no. 1, p. 3, 2022, doi: 10.3390/app13010003.

[7] J. Lee, C. Yeo, K. C. Bae, and D. Mun, 'Replacing NURBS surfaces with analytic surfaces based on isocurve characteristics in B-rep models', *J. Comput. Des. Eng.*, vol. 12, no. 8, pp. 78–106, 2025, doi: 10.1093/jcde/qwaf063.

[8] S. Samreen, M. Sarfraz, and A. Mohamed, 'A quadratic trigonometric B-Spline as an alternate to cubic B-spline', *Alex. Eng. J.*, vol. 61, no. 12, pp. 11433–11443, 2022, doi: 10.1016/j.aej.2022.05.006.

[9] Y. Yan, G. He, C. Yao, S. Wang, and Z. Tan, 'A precision reconstruction method based on refined and adjusted multilevel T-spline for complex surface manufacturing', *J. Manuf. Process.*, vol. 153, pp. 531–546, 2025, doi: 10.1016/j.jmapro.2025.08.070.

[10] C. Harmening and R. Butzer, 'Improving the approximation quality of tensor product B-spline surfaces by local parameterization', *J. Appl. Geod.*, vol. 18, no. 4, pp. 575–596, 2024, doi: 10.1515/jag-2023-0071.

[11] P. Cong, D. Zhou, W. Li, and M. Deng, 'Structural optimization of mining decanter centrifuge based on response surface method and multi-objective genetic algorithm', *Chem. Eng. Process. - Process Intensif.*, vol. 212, p. 110276, 2025, doi: 10.1016/j.cep.2025.110276.

[12] Y. T. Wibowo, N. Siswanto, and M. Suef, 'Response surface methodology approach in achieving multi-response setup optimization in the machining process', *Salud Cienc. Tecnol.*, vol. 2, p. 190, 2022, doi: 10.56294/saludcyt2022190.

[13] N. Szpisják-Gulyás, A. N. Al-Tayawi, Zs. H. Horváth, Zs. László, Sz. Kertész, and C. Hodúr, 'Methods for experimental design, central composite design and the Box–Behnken design, to optimise operational parameters: A review', *Acta Aliment.*, vol. 52, no. 4, pp. 521–537, 2023, doi: 10.1556/066.2023.00235.

[14] C. Lu and J. Shi, 'Relative density and surface roughness prediction for Inconel 718 by selective laser melting: central composite design and multi-objective optimization', *Int. J. Adv. Manuf. Technol.*, vol. 119, no. 5–6, pp. 3931–3949, 2022, doi: 10.1007/s00170-021-08388-2.

[15] M. Ben Said, E. Ftoutou, I. Hajjaji, A. Benkhalifa, and M. Trigui, 'Experimental investigations of tooth pitch variation and cutting parameters on areal surface texture in flat end milling of Fe–Ni alloy Supra50', *Int. J. Adv. Manuf. Technol.*, vol. 139, no. 9–10, pp. 5009–5023, 2025, doi: 10.1007/s00170-025-16210-6.

[16] B. He, S. Ding, and Z. Shi, 'A comparison between profile and areal surface roughness parameters', *Metrol. Meas. Syst.*, pp. 413–438, 2021, doi: 10.24425/mms.2021.137133.

[17] M. Raza, Z. Alam, and A. D. Udai, 'ISO Standardized Form Removal and Filtering of Surface Texture for Areal Surface Roughness Measurement Using Zygo Mx', *MAPAN*, vol. 40, no. 4, pp. 937–942, 2025, doi: 10.1007/s12647-025-00844-8.

[18] I. Malkorra *et al.*, 'Numerical modelling of the drag finishing process at a macroscopic scale to optimize surface roughness improvement on additively manufactured (SLM) Inconel 718 parts', *Procedia CIRP*, vol. 108, pp. 648–653, 2022, doi: 10.1016/j.procir.2022.01.002.

[19] J. Kalisz, K. Żak, S. Wojciechowski, M. K. Gupta, and G. M. Krolczyk, 'Technological and tribological aspects of milling-burnishing process of complex surfaces', *Tribol. Int.*, vol. 155, p. 106770, 2021, doi: 10.1016/j.triboint.2020.106770.

[20] R. Adhikari, G. Bolar, R. Shanmugam, and U. Koklu, 'Machinability and surface integrity investigation during helical hole milling in AZ31 magnesium alloy', *Int. J. Lightweight Mater. Manuf.*, vol. 6, no. 2, pp. 149–164, 2023, doi: 10.1016/j.ijlmm.2022.09.006.

[21] Muhamad Afiq Azwan Yusni, N. K. Kamardin, A. F. Zubair, and A. S. Mohd Rodzi, 'The Effects Of Taguchi Method And Anova In Optimizing Parameters For Enhancing Power Optimization For Electrical Discharge', *J. Mek.*, 2025, doi: 10.11113/jm.v48.563.

[22] A. F. Zubair and M. S. Abu Mansor, 'Embedding firefly algorithm in optimization of CAPP turning machining parameters for cutting tool selections', *Comput. Ind. Eng.*, vol. 135, pp. 317–325, 2019, doi: 10.1016/j.cie.2019.06.006.

[23] Y. Yang and X. Wei, 'Optimization of Process Parameters for Surface Roughness and Milling Power of AL7075 CNC Milling Based on a Hybrid Multi-Objective Particle Swarm Optimization Integrating Whale Optimization Algorithm', *Integrating Mater. Manuf. Innov.*, vol. 14, no. 3, pp. 401–424, 2025, doi: 10.1007/s40192-025-00412-7.

[24] Assab, 'Stavax ESR (2024)'. [Online]. Available: https://www.assab.com/app/uploads/sites/199/2024/05/Stavax_ESR_PH-EN.pdf

[25] Z. Xie *et al.*, 'The manufacturing process and influencing factors for curved aspheric-microlens arrays by Slow Tool Servo Machining', *J. Manuf. Process.*, vol. 125, pp. 217–225, 2024, doi: 10.1016/j.jmapro.2024.07.032.

[26] Y. Sun, Z. He, C. Fu, Z. Xie, B. Zhang, and H. Liu, 'Surface modeling and influencing factors for microlens array by slow tool servo machining', *J. Manuf. Process.*, vol. 102, pp. 365–374, 2023, doi: 10.1016/j.jmapro.2023.07.037.

[27] W. Ji, H. Shang, B. Li, H. Yang, and Z. Li, 'Effects of tool orientation and surface curvature on tool wear in ball end milling of 17-4PH stainless steel', *Int. J. Adv. Manuf. Technol.*, vol. 135, no. 11–12, pp. 5595–5613, 2024, doi: 10.1007/s00170-024-14836-6.

[28] L. L. Duan, G. Y. Yang, D. C. Hao, F. Huang, J. Xing, and K. X. Liu, 'Tribological and Mechanical Properties of Nanocrystalline TiN, TiAlN, and TiSiN PVD Coatings', *Strength Mater.*, vol. 55, no. 4, pp. 822–833, 2023, doi: 10.1007/s11223-023-00573-w.

[29] N. Geier and C. Pereszlai, 'Analysis of characteristics of surface roughness of machined CFRP composites', *Period. Polytech. Mech. Eng.*, vol. 64, no. 1, pp. 67–80, 2020, doi: 10.3311/PPme.14436.

[30] T. Pavol, J. Holubjak, V. Bechný, M. Novák, A. Czán, and T. Czánová, 'Surface Analysis and Digitization of Components Manufactured by SLM and ADAM Additive Technologies', *Manuf. Technol.*, vol. 23, no. 1, pp. 127–134, 2023, doi: 10.21062/mft.2023.008.

[31] A. Pereira, M. Fenollera, T. Prado, and M. Wieczorowski, 'Effect of Surface Texture on the Structural Adhesive Joining Properties of Aluminum 7075 and TEPEX®', *Materials*, vol. 15, no. 3, 2022, doi: 10.3390/ma15030887.

[32] M. Vanrusselt, H. Haitjema, R. Leach, and P. De Groot, 'International comparison of flatness deviation in areal surface topography measurements', *CIRP Ann.*, vol. 71, no. 1, pp. 453–456, 2022, doi: 10.1016/j.cirp.2022.04.030.

[33] M. K N, B. Hosamani, Nagaraju, V. Kemminje, V. R. Raju, and Nagahanumaiah, 'An investigation into the surface integrity and cutting force characteristics in titanium alloy end milling using soluble oil and MQL as coolants', *Results Surf. Interfaces*, vol. 17, p. 100341, 2024, doi: 10.1016/j.rsurfi.2024.100341.

[34] J. Wang, C. Zhang, F. Jiao, and Y. Cao, 'Parameters optimization for 2.5D needled Cf/SiC in longitudinal torsional ultrasonic-assisted laser milling on PSO-BP-PSO', *CIRP J. Manuf. Sci. Technol.*, vol. 58, pp. 87–106, 2025, doi: 10.1016/j.cirpj.2025.02.002.

© 2026 by the authors. Submitted for possible open access publication under the terms and conditions of the Creative Commons Attribution (CC BY-NC-ND) license (http://creativecommons.org/licenses/by/4.0/).